J. Synchrotron Rad. (2000). **7**, 12–17

Performance limits of direct cryogenically cooled silicon monochromators – experimental results at the APS

Wah-Keat Lee,* Patricia Fernandez and Dennis M. Mills

Advanced Photon Source, Argonne National Laboratory, 9700 South Cass Avenue, Argonne, IL 60439, USA. E-mail: wklee@aps.anl.gov

(*Received 5 October 1999; accepted 8 November 1999*)

The successful use of cryogenically cooled silicon monochromators at third-generation synchrotron facilities is well documented. At the Advanced Photon Source (APS) it has been shown that, at 100 mA operation with the standard APS undulator A, the cryogenically cooled silicon monochromator performs very well with minimal (<2 arcsec) or no observable thermal distortions. However, to date there has not been any systematic experimental study on the performance limits of this approach. This paper presents experimental results on the performance limits of these directly cooled crystals. The results show that if the beam is limited to the size of the radiation central cone then, at the APS, the crystal will still perform well at twice the present 100 mA single 2.4 m-long 3.3 cm-period undulator heat load. However, the performance would degrade rapidly if a much larger incident white-beam size is utilized.

Keywords: X-ray optics; high-heat-load optics; cryogenic cooling; silicon monochromators.

1. Introduction

Insertion devices at third-generation synchrotron sources are capable of producing X-ray beams with very high power and power densities. X-ray optics subjected to these intense beams will develop severe strains or sometimes even fracture or melt, unless they are properly cooled. One successful approach to this heat-load problem has been the use of cryogenic cooling.

The implementation and successful tests of cryogenically cooled silicon monochromators at third-generation synchrotron sources are well documented (Holmberg, 1994; Marot, 1995; Rogers *et al.*, 1995; Rogers, Mills, Fernandez *et al.*, 1996; Rogers, Mills, Lee *et al.*, 1996). In particular, it has been shown that at the Advanced Photon Source (APS), with 100 mA storage-ring current and the standard 2.4 m-long 3.3 cm-period APS undulator A, the cryogenically cooled silicon monochromator performs very well with minimal (<2 arcsec) or no observable thermal distortions (Rogers, Mills, Lee *et al.*, 1996). Currently, cryogenically cooled silicon monochromators are being used at several beamlines at both the APS and the European Synchrotron Research Facility (ESRF).

Although this approach has been successful with the current APS and ESRF heat loads, there has not been any published experimental investigation into its performance limits. At the APS the straight sections in the storage ring are 5 m long and thus can accommodate two 2.4 m-long (or one 5 m-long) insertion devices. Furthermore, there is the possibility of operating the machine at currents higher than 100 mA. Therefore, it is of interest to see if the beamline components, such as the monochromator, can handle the increased heat load. The goal of this study is to investigate the performance limits of the direct cryogenically cooled silicon monochromators and from them obtain quantitative estimates for its performance under different heat-load conditions.

Finite-element-analysis (FEA) modelling of the cryogenically cooled crystals has proved to be quite challenging due to the highly nonlinear nature (as a function of temperature) of the thermal and mechanical properties of silicon at cryogenic temperatures. Fig. 1 shows the strong and nonlinear temperature dependence on the figure of merit [k/α, where k is the thermal conductivity ($\mathrm{W\ cm^{-1}\ K^{-1}}$) and α is the thermal expansion coefficient ($\mathrm{K^{-1}}$)]. Finite-element calculations performed at the APS have shown that small differences in the model, mesh density or cell sizes can result in considerably different crystal distortions. Zhang (1993) has performed detailed finite-element calculations on cryogenically cooled monochromators. His study, however, is for contact-cooled crystals and also assumes that the entire heat load is absorbed at the crystal surface. The results of the measurements presented here will show that this assumption is not valid, and that in fact the actual depth profile of the absorbed power is very important.

Recently, an additional undulator was temporarily installed in the APS sector 1-ID straight section. The two undulators in tandem provided an excellent opportunity to perform high-heat-load optics experiments at up to twice the normal power loads. Both direct cryogenically cooled silicon and room-temperature diamond monochromators were studied. This paper will only present the results of the cryogenic silicon monochromator.

© 2000 International Union of Crystallography
Printed in Great Britain – all rights reserved

2. Experimental details

The experimental setup for the measurements on the APS 1-ID beamline described in this paper is shown in Fig. 2. The 'normal' undulator was located at the downstream end of the 5 m-long straight section, while the 'new' undulator was inserted at the upstream end of the straight section. Both are the standard APS 2.4 m-long 3.3 cm-period undulator A. For convenience the upstream undulator will be denoted as UA1 and the downstream undulator as UA2. The distance from the center of UA1 to the center of the white-beam slit assembly is 29.17 m, while the corresponding distance for UA2 is 26.67 m. A window, consisting of two 0.25 mm-thick cooled Be foils, isolates the storage ring and front-end vacuum from the downstream side. The upstream apertures limit the size of the white beam incident on the window to ~3 mm (H) × 2 mm (V). The distance between the white-beam slits and the double-crystal monochromator (DCM) is ~1.5 m. The ion chambers were located in 1-ID-C station, which is ~30 m from the DCM.

Measurements were performed with the 'standard' APS cryogenic silicon crystal, as shown in Fig. 3. The crystal surface was parallel to the Si(111) planes. Measurements were made on both the thin and the thick parts of the crystal, as marked in Fig. 3. Note that this crystal is different from the crystals used in previous publications (Rogers *et al.*, 1995; Rogers, Mills, Fernandez *et al.*, 1996; Rogers, Mills, Lee *et al.*, 1996). In particular, the thin web of the crystal is considerably different in dimensions and construction. The reason for the difference is due to fabrication difficulties of the previous design. The previous design had the thin diffracting web sitting in a small trough/groove; the lateral dimension of the trough/groove was carefully matched to the lateral beam size. The tight space constraint hampered the lapping and polishing of the thin web. This current design solves the fabrication problems but, as will be discussed later, at a price of poor thermal performance.

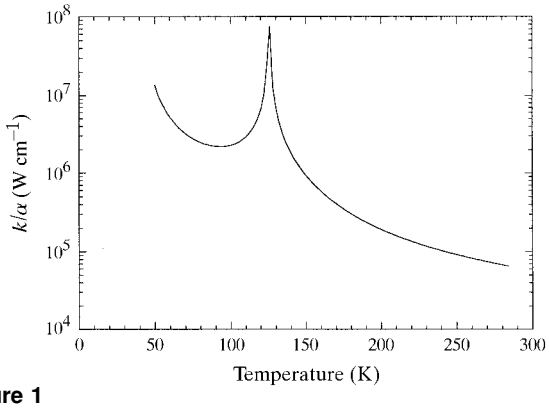

Figure 1
Figure of merit, k/α (W cm^{-1}), of silicon as a function of temperature (K). α is the thermal expansion coefficient (K^{-1}) and k is the thermal conductivity (W cm^{-1} K^{-1}).

Double-crystal rocking-curve measurements were performed by rotating the second crystal of the DCM with a piezoelectric device. The ion chambers I0 and I1 detect the monochromatic beam intensity from the DCM. By using appropriate filters between the two ion chambers, I1 detects the higher-energy photons from high-order reflections, such as Si(333). Within the range of the measurements presented here, the theoretical rocking-curve widths of these high-energy high-order reflections are less than 1 arcsec. Thus, the width of the I1 rocking curve is very sensitive to thermal distortions. Open-gap or 'cold-beam' measurements show that the I1 rocking-curve width varies from 0.5 to 2.0 arcsec, depending on the angle, beam size and location of the beam footprint. These measurements show that the residual mounting/fabrication-induced strains on the crystal are relatively small.

The thin part of the crystal has the advantage of only absorbing a fraction of the total incoming beam power but has the disadvantage of a reduced thermal dissipation path. Conversely, the thick crystal has a better thermal dissipation path but also absorbs more of the incoming beam power. Measurements were made for several different white-beam slit settings: from 1.5 mm (H) × 0.5 mm (V) to 3.0 mm (H) × 2.0 mm (V). The 1.5 mm (H) × 0.5 mm (V) white-beam setting corresponds to the full width at half-maximum (FWHM) of the undulator odd-harmonic central cone. The 3.0 mm (H) × 2.0 mm (V) white-beam setting corresponds to the size of the upstream aperture/window.

Two types of measurements were generally performed: (i) at fixed energy (mostly at 8 and 20 keV), varying the undulator gap(s), and (ii) at different energies (7–20 keV), tuning the undulator to the appropriate gap(s) for maximum flux. The first type of measurement is useful for thermal calculations since varying the gaps is an easy way to control the incident power (although the spectral and

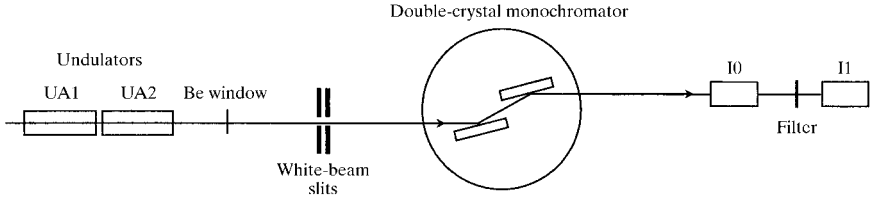

Figure 2
Schematic diagram of the experimental setup (not to scale). Distances from UA1 and UA2 centers to the white-beam slits are 29.17 m and 26.67 m, respectively. The distance from the white-beam slits to the DCM is ~1.5 m. The distance from the ion chambers to the DCM is ~30 m.

spatial distribution changes too), while the second type of measurement is how a beamline user would normally operate the DCM/undulator. The liquid N_2 (LN2) flow rate was held between 6.4 and 8.4 l min^{-1} throughout most of the measurements. The flow rate corresponds to a flow velocity of ~190–250 cm s^{-1}.

Incident and absorbed power calculations were performed using the *XUS* and *XPOWER* codes which have been bundled into a graphical interface program called *XOP* (Dejus & del Rio, 1996). The calculations assume the slit blades are at the center of the slit assembly, even though, in reality, the horizontal blades are slightly upstream and the vertical blades are slightly downstream of the center of the slit assembly. Calorimetry measurements were performed as a check for the calculations. Table 1 shows the calculated and measured incident powers on the crystal at a 100 mA ring current, with a 3 mm (H) × 2 mm (V) white-beam slit size. The measurements are within ~10% of the calculated values for the high-power cases, which is more important here. The measurements are in less agreement (~20–25%) with calculations at lower powers. (Note: at the same gap, UA2 delivers more power through the white-beam slits because it is 2.5 m closer to the slits than UA1.) Beam collinearity of the two undulators was measured to be within 0.5 mm of each other at the experimental station in 1-ID-C, which is 30 m from the DCM. This, together with the power measurements, show that the two undulators were well aligned.

Table 1
Calculated and measured white-beam power for various undulator gaps at 100 mA.

The white-beam slit size was 3 mm (H) × 2 mm (V).

UA1 gap (mm)	UA2 gap (mm)	Calculated power (W)	Measured power (W)
20	50	263	195
50	20	299	241
20	20	562	437
11	50	753	695
50	11	881	773

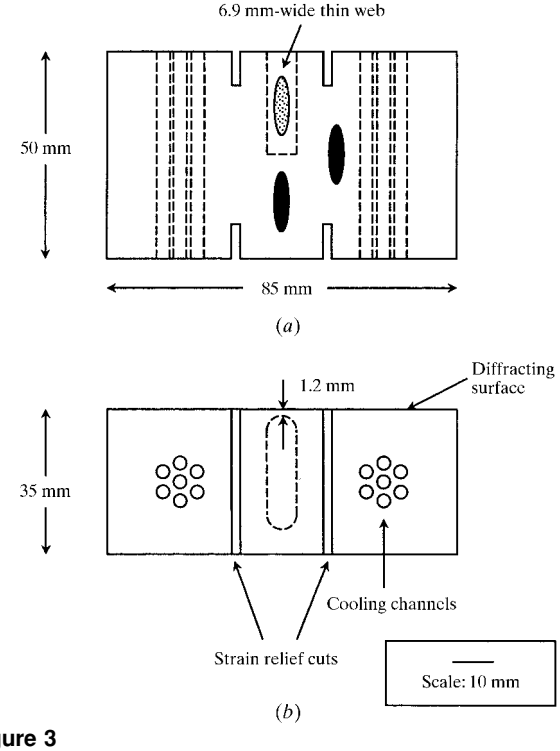

Figure 3
Schematic diagram of the crystal used in this paper. (*a*) Top view. (*b*) Edge view, looking downstream. Note that, unlike previous crystals, this one has a flat top for easier fabrication. The dotted oval indicates the approximate position of the beam footprint for the thin-crystal measurements, and the dark filled ovals indicate the beam footprint positions for the thick-crystal measurements. The thinnest portion of the thin web is ~1.2 mm. As in previous crystals, sealing is accomplished with indium foils and metal c-rings. The drawing is approximately to scale.

3. Results

Before presenting the results of the experiment it is useful to discuss several pertinent issues that will explain the rationale behind the data plots. The focus of this paper is to investigate the performance limits of this monochromator and to provide quantitative estimates for its performance under different heat-load conditions. To do this one needs to identify the thermal variable(s) that drive the thermal distortions.

For a simple model (crystal block, heated from above and cooled from below) in which all the power is absorbed on the crystal surface, it can be shown (Subbotin *et al.*, 1988) that $\Delta\theta \propto Q\alpha/k$, where $\Delta\theta$ is the thermal-induced slope error, Q is the absorbed heat flux or surface power density (W mm^{-2}) and α/k is the inverse of the figure of merit plotted in Fig. 1.

α/k is dependent on the temperature. Therefore, the total absorbed power, which directly affects the average crystal temperature, must be one of the thermal variables that drives the thermal distortions. The above simple model also suggests that the power density must be another thermal variable that drives the thermal distortions. In the above model in which all the power is absorbed on the surface, Q may be identified with the surface power density. However, in reality, owing to the high critical energy of the radiation, the power is not all absorbed at the crystal surface. Under closed-gap (11 mm) conditions, ~50% of the incident power is absorbed at distances of greater than 2 mm from the surface (measured along the beam direction). The identification of Q with a 'real' situation thermal variable is thus not straightforward. Based on the extinction lengths in the range of our measurement parameters (several microns), one possibility is to associate Q with the average absorbed power density in the first 10 μm (measured along the beam path) of the crystal; *i.e.* the power absorbed in the first 10 μm divided by the beam footprint. Thus, instead of a surface power density (W mm^{-2}) we consider an average

power density (W mm^{-2}) within the first 10 μm. Owing to the high critical energy of the radiation, the absorption lengths are in the millimeter range. Therefore, the differences in the average power density within the first few tens of microns are small. Thus, one does not need to consider the average power density within the exact extinction length for each case. The data analysis will show that the choice of this thermal variable appears reasonable.

Fig. 4 shows a plot of the measured I1 FWHM against the two variables: total absorbed power and average absorbed power density in the first 10 μm (measured along the beam path) of the crystal for the thick crystal case. The power and power density values were calculated using *XUS* and *XPOWER* programs under *XOP* (Dejus & del Rio, 1996). Since the measured power is ∼10% lower (in the high-power regime) and the calculations do not include Compton scattering losses (a 10% effect here), the 'true' power and power density values on the axes may be off by as much as 20%. The data are a collection of all the measurements performed during the double-undulator runs, including data at various energies and slit sizes. The different symbols of the data points indicate the different measured I1 FWHMs, as described in the figure caption. For example, the filled triangle point in the right-most part of the plot is the data for the case in which the total absorbed power in the crystal was 1368 W, the average absorbed power density in the first 10 μm of the crystal was 2.2 W mm^{-2}, and the measured I1 FWHM was 49 arcsec.

The hyperbolic-like curve in Fig. 4 is a guide to the eye: the data suggest that, if the heat variables fall to the left and below this curve, the crystal should have less than 2 arcsec thermal distortion (from the fact that almost all data points in the plot to the left and below this line have a measured I1 FWHM of 2 arcsec or less.) A typical user would normally tune the undulator so that the desired energy is an odd harmonic of the undulator. In the 7–20 keV range this is either the first or third harmonic of the undulator. Normally, the first harmonic would be used in the 7–12 keV range, and the third harmonic would be used in the 12–20 keV range. Assuming such a mode of operation, one can plot these 'heat-load tuning curves' to trace the total power absorbed and the average power density absorbed in the first 10 μm of silicon as the undulator and monochromator are tuned through these energies (7–20 keV). These heat-load tuning curves are drawn in as lines in Fig. 4 for two different white-beam slit sizes: 3 mm (H) × 2 mm (V) and 1.5 mm (H) × 0.5 mm (V) at 26.67 m from the source. The smaller slit is approximately the size of the central radiation cone for an odd harmonic at the white-beam slit location and is typical of the beam sizes used by users. The heat-load tuning curves are drawn for both 100 mA and 200 mA ring current, assuming a single 2.4 m-long undulator. Note that the peak of the heat-load tuning curve is higher for the smaller slit. This is simply because with a smaller slit the average absorbed power density approaches the peak absorbed power density.

Fig. 4 shows that, with a large beam size [3 mm (H) × 2 mm (V)], the thick crystal will perform well at 100 mA but not at 200 mA. On the other hand, if the beam size is reduced, using slits, to its central cone value of 1.5 mm (H) × 0.5 mm (V) at 26.67 m, then this crystal will still work at 200 mA (single undulator).

In order to appreciate the dramatic change in rocking-curve width with the thermal load, Fig. 5 is a three-dimensional surface plot of the same data. The x and y axes represent the thermal variables as in Fig. 4, and the z axis represents the measured I1 FWHM. This plot shows how dramatically the thermal distortions change as a function of the thermal load, as expected from Fig. 1, due to the temperature dependence of α/k for silicon. With increasing heat load, the overall temperature of the crystal increases.

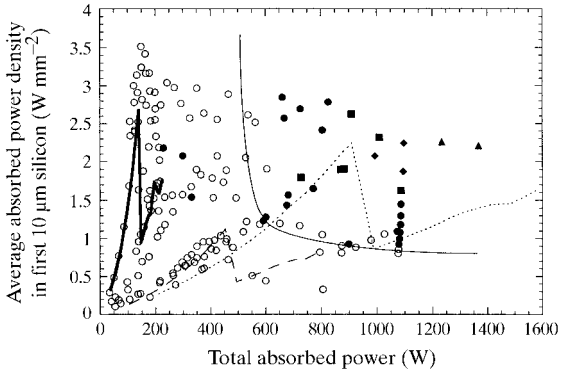

Figure 4
A plot of all the data collected on the thick part of the crystal. The symbols represent the following: open circles, I1 FWHM < 2″; filled circles, 2″ < I1 FWHM < 10″; filled squares, 10″ < I1 FWHM < 20″; filled diamonds, 20″ < I1 FWHM < 30″; filled triangles, I1 FWHM > 30″. The hyperbolic-like curve is a guide to the eye: the data suggest that, for heat-load variables to the left and below this curve, the thermal distortions will be less than 2″. Three 'heat-load tuning curves' are also shown. Dashed line: 3 mm (H) × 2 mm (V) white-beam single undulator, 100 mA ring current; dotted line: 3 mm (H) × 2 mm (V) white-beam single undulator, 200 mA ring current; thick solid line: 1.5 mm (H) × 0.5 mm (V) white-beam single undulator, 200 mA ring current.

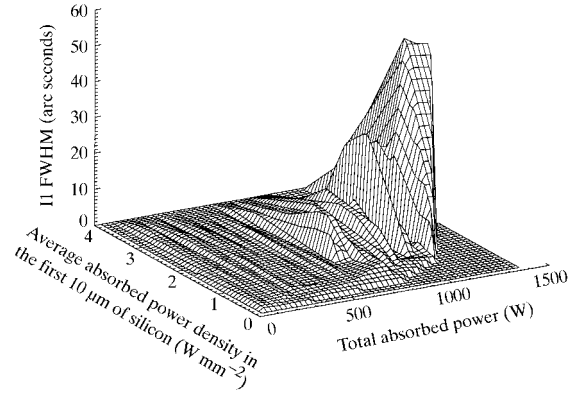

Figure 5
A three-dimensional rendition of the data from Fig. 4 showing the rapid rise in thermal distortions. This figure was drawn using *IDL*, which interpolates the data and creates a 'solid' surface.

If the overall temperature of the crystal remains in the cryogenic range, the thermomechanical properties of the crystal remain very good and a small additional local heat load on the crystal will result in little or no thermal distortions. However, with increasing heat load the overall temperature of the crystal increases. If the overall temperature increases beyond the cryogenic regime, then the thermomechanical properties of the crystal deteriorate rapidly, and the same small additional heat load on the crystal will result in large structural distortions. Owing to the nonlinear temperature dependence of α/k in the cryogenic regime, this transition happens rapidly.

Fig. 6 shows a plot of the I1 FWHM *versus* total absorbed power and the average absorbed power density in the first 10 μm of silicon for the thin crystal case. Note the difference in the horizontal scale between Figs. 4 and 6 because the thin crystal absorbs less of the total incident power. Similar heat-load tuning curves and the guide to the eye are drawn.

Comparing Figs. 4 and 6 it is clear that for this crystal the performance with the beam on the thin part of the crystal is considerably worse than that with the beam on the thick part. In fact, the thin crystal does not work [3 mm (H) × 2 mm (V)] even with just a single undulator at 100 mA operation. This result may seem to contradict previous results (Rogers, Mills, Lee *et al.*, 1996), but we wish to reiterate and emphasize that the 'thin' crystals used previously were of an entirely different design. Knapp *et al.* (1994) have shown that, for the original thin crystal design, careful matching of the dimensions of the thin web and the dimensions of the beam were critical in determining whether the crystal would work. The thin crystal used here was designed for ease of fabrication with no detailed consideration of its would-be thermal performance, with the idea that it would be tested experimentally once installed on the beamline.

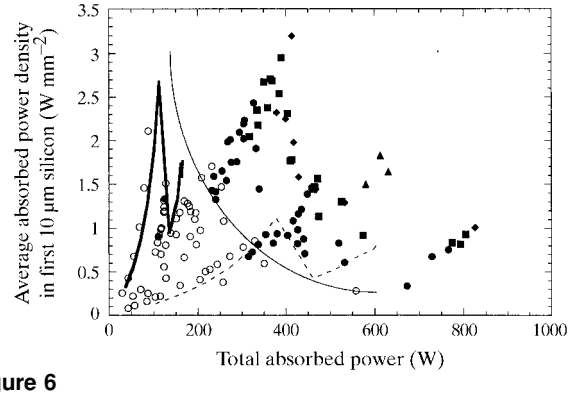

Figure 6
A plot of all the data collected on the thin part of the crystal. The symbols represent the following: open circles, I1 FWHM < 2″; filled circles, 2″ < I1 FWHM < 10″; filled squares, 10″ < I1 FWHM < 20″; filled diamonds, 20″ < I1 FWHM < 30″; filled triangles, I1 FWHM > 30″. The hyperbolic-like curve is a guide to the eye: the data suggest that, for heat-load variables to the left and below this curve, the thermal distortions will be less than 2″. Two 'heat-load tuning curves' are also shown. Dashed line: 3 mm (H) × 2 mm (V) white-beam single undulator, 100 mA ring current; thick solid line: 1.5 mm (H) × 0.5 mm (V) white-beam single undulator, 200 mA ring current.

Table 2
Comparison of the thermal distortion for the same total absorbed power but different absorption profile.

Data were collected at the same white-beam slit size and crystal angle on the thick part of the crystal.

UA1 (mm)	UA2 (mm)	Total absorbed power (W)	Total absorbed power in first 10 μm of crystal (W)	Measured I1 FWHM (arcsec)
Open	11	874	22	1.6
17	17	882	46	15.7

Fig. 6 also shows that, for a small beam size [1.5 mm (H) × 0.5 mm (V)], the thin crystal may still work at a ring current up to 200 mA. The comparative performance between the thin and thick crystals can be understood as follows. For the thin crystal, the ability to conduct away the heat is significantly reduced. For low absorbed powers (<150 W), the average temperature of the thin web remains in the cryogenic regime, and thus the thermomechanical properties of the crystal remain very good. Therefore, in this low-absorbed-power regime, the thin crystal performs as well as the thick crystal. As the absorbed power increases, however, the reduced thermal dissipation path of the thin crystal causes its average temperature to rise quickly, compared with the thick crystal. The higher temperature causes the thermomechanical properties of the crystal to deteriorate rapidly, and the thermal distortions become significantly larger than for the thick crystal.

One final remark to be made here is that the power absorption profile in the crystal is an important parameter in determining the thermal distortions. This is clearly illustrated in Table 2. Table 2 shows thick-crystal data taken with the same white-beam slit size [3 mm (H) × 2 mm (V)] and crystal angle. For the same total absorbed power, the thermal distortions differ considerably depending on the actual amount of power absorbed in the first 10 μm of silicon. The difference in this surface absorption is due to the higher critical energy of the beam in the 11 mm-gap case compared with that of the 17 mm-gap case.

In conclusion, this paper presents experimental results showing the performance limits of direct cryogenically cooled silicon monochromators. The results show that, in considering the effect of a certain heat load on the crystal in addition to the total absorbed power, the actual power-absorption profile plays an important role in determining the thermal distortions. In particular, the average absorbed power density in the first few tens of microns is important. The results show that the current cryogenically cooled silicon monochromator can handle the heat load from either a single undulator, 200 mA operation, or a double undulator, 100 mA operation, at the APS. Useful guides to predicting the performance of the crystal have also been provided.

We wish to thank Felix Krasnicky and Josef Maj for their assistance in fabrication and characterization of the crystals, and the SRICAT sector 1 staff for their assistance on the beamline. This work has been supported by the US Department of Energy, BES-Materials Science under contract No. W-31-109-ENG-38.

References

Dejus, R. J. & del Rio, M. S. (1996). *Rev. Sci. Instrum.* **67**(9). CD-ROM.

Holmberg, J. (1994). *Workshop on Thermal Management of X-ray Optical Components for Synchrotron Radiation*, Advanced Photon Source, Argonne, IL, USA.

Knapp, G. S., Beno, M. A., Rogers, C. S., Wiley, C. L. & Cowan, P. L. (1994). *Rev. Sci. Instrum.* **65**(9), 2792–2797.

Marot, G. (1995). *Opt. Eng.* **34**(2), 426–431.

Rogers, C. S., Mills, D. M., Fernandez, P. B., Knapp, G. S., Wulff, M., Rossat, M., Hanfland, M. & Yamaoka, H. (1996). *Rev. Sci. Instrum.* **67**(9). CD-ROM.

Rogers, C. S., Mills, D. M., Lee, W. K., Fernandez, P. B. & Graber, T. (1996). *Proc. SPIE*, **2855**, 170–179.

Rogers, C. S., Mills, D. M., Lee, W. K., Knapp, G. S., Holmberg, J., Freund, A., Wulff, M., Rossat, M., Hanfland, M. & Yamaoka, H. (1995). *Rev. Sci. Instrum.* **66**(6), 3494–3499.

Subbotin, V. I., Kolesov, V. S., Kuz Min, Yu. A. & Kharitonov, V. V. (1988). *Sov. Phys. Dokl.* **33**(8), 633–635.

Zhang, L. (1993). *Proc. SPIE*, **1997**, 223–235.